PROCEEDINGS OF SCIENCE

Dark Matter Limits from the CALET Electron+Positron Spectrum with Individual Astrophysical Source Background

Holger Motz[a,*] **for the CALET collaboration**

[a] *Kanagawa University, 3-27-1 Rokkakubashi, Kanagawa, Yokohama, Kanagawa 221-8686, Japan*

E-mail: motz@aoni.waseda.jp

The ISS-based Calorimetric Electron Telescope (CALET) is directly measuring the energy spectrum of electron+positron cosmic rays up to 20 TeV. Annihilation or decay of dark matter (DM) could produce signatures in the positron and electron cosmic-ray spectra, thus the parameter space of DM candidate models can be probed by studying these messengers. The TeV-region extension of the spectrum provided by CALET is especially important for heavy DM search, since the signature's location in energy is closely correlated with the DM mass. The magnet spectrometer AMS-02 on the other hand provides an exclusive positron-only spectrum below the TeV range. The combined analysis of both data-sets allows for DM search with a sophisticated modeling of the astrophysical background, comprising pulsars as the primary positron source and supernova remnant (SNR) sources providing the majority of the electron flux, in addition to a secondary component. As a refinement over a phenomenological power-law parametrization of the background, overlapping individual point source spectra are used as background for deriving limits on DM annihilation and decay from the CALET all-electron and the AMS-02 positron-only data. The used SNR and pulsar samples combine known nearby sources dominating the spectrum at high energies with randomly generated ones throughout the galaxy. By analyzing a large number of samples with also randomized emission spectra parameters, the expected variability of the background is taken into account, improving the reliability of the obtained limits on DM annihilation cross-section and lifetime.

38th International Cosmic Ray Conference (ICRC2023)
26 July - 3 August, 2023
Nagoya, Japan

*Speaker

PoS(ICRC2023)1385

1. Introduction

Limits on DM annihilation and decay have been derived from the all-electron (electron+positron) spectrum measured by CALET [1], and the positron spectrum from AMS-02 [2]. The astrophysical background for the positron spectrum is limited to pulsars and secondary particles, but it reaches only up to 1 TeV, while the background for the all-electron spectrum which extends up to 4.8 TeV includes also SNRs. This work improves over previously used methods [3–6], in that all the primary astrophysical background is calculated as the overlapping spectra from randomly generated populations of SNRs and pulsars throughout the galaxy, replicating the spectral structures expected from this origin. This addresses the issue of assuming a potentially too smooth background spectrum in the case of a power law parametrization for all or part of the SNR and pulsar populations.

2. Astrophysical Base Model

Calculation of the limits on annihilation cross section or livetime is based on the reduction of the fit quality when adding the predicted DM signal to a purely astrophysical base model which fits the data well. To construct this base model, the CALET dataset [1] over the full energy range from 10.6 GeV to 4.8 TeV, and the AMS-02 positron-only dataset [2] from 2 GeV to 1 TeV, are fitted with functions comprised of the overlapping spectra from individual point-sources (SNRs and pulsars), where the free parameters are the average source spectrum power-law indices ($\gamma_{i(SNR)}$ and $\gamma_{i(pulsar)}$), cut-off energies ($E_{cut(SNR)}$ and $E_{cut(pulsar)}$), and the average efficiencies at which electron cosmic rays are accelerated by the SNRs and pulsars ($\eta_{(SNR)}$ and $\eta_{(pulsar)}$). To account for the variability of the astrophysical background, 80 random samples of the SNRs and pulsars expected within the galaxy over the past 200 Myr have been created for use as the base model. The spatial distribution of supernovae is taken from Ref. [7], with a supernova rate of 2.1 per 100 years, and the birth rate of the associated pulsars is set to 1.7 per 100 years following Ref. [8]. The resulting samples are comprised of over 4 million SNRs and 3 million pulsars each. For the kinetic energy of the supernovae, the values of $log_{10}(E_{SNR}/\mathrm{erg})$ are drawn from a normal distribution with mean 51 and width 1, and a hard cut-off at 5×10^{52} erg. The initial rotation energy of pulsars, is determined by drawing $log_{10}(E_{pulsar}/\mathrm{erg})$ from a normal distribution with mean 49.30 and width 1.01, which are obtained from a fit to the energies of the pulsars in the ATNF catalog [9]. Furthermore, within each sample, the source spectrum power-law indices are varied randomly following a normal distribution of width 0.033, while log_{10} of the efficiencies is varied following a normal distribution of width 0.33, each cut off at 3σ. Propagation is calculated by the semi-analytical method established in Ref. [10]. The parameters governing propagation are taken from the model explained in Ref. [11], based on matching the output of calculations of the spallation network with DRAGON to the measured nuclei spectra under the assumption that all nuclei species share a common power law with cut-off source spectrum and the structures (hardening, softening) in the observed spectra are due to propagation effects. In addition to above primary astrophysical sources, the flux of secondary electrons and positrons is included, which is taken from the DRAGON nuclei spectra calculations used to define the propagation model [11]. Solar modulation is treated by the force-field approximation with an

energy and charge-sign dependent potential inspired by Ref. [12] given by

$$\Phi(R) = \Phi_0 + \Phi_{1\pm}\frac{1+(R/R_r)^2}{(R/R_r)^3}\ , \tag{1}$$

introducing the base potential Φ_0, the additional potentials Φ_{1+} and Φ_{1-} for positively and negatively charged particles respectively, as well as the reference rigidity R_r as additional fit parameters. For CALET data, the energy dependent 1σ deviation $\Delta(E)$ is calculated for each data point in the same way as the values listed in the supplemental material of Ref. [13] for the following systematic uncertainty sources: Normalization, tracking, charge selection, electron identification, Monte Carlo model dependence. A shift by $w\Delta(E)$ is performed as part of the fit function (represented by a gray band in Fig. 1 and Fig. 3) with the weight w for each systematic uncertainty source as a free parameter and each squared weight added to the total χ^2 of the fit as explained in Ref. [4]. Further details on this interpretation of the CALET and AMS-02 spectra by astrophysical sources and results on the source properties are given in Ref. [14].

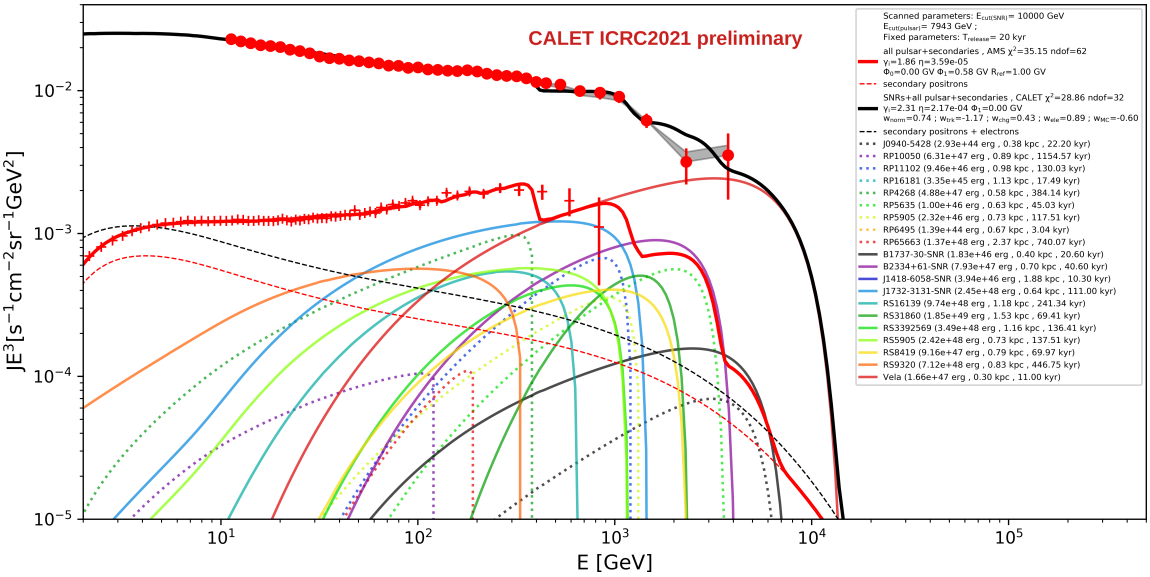

Figure 1: Base model fit for one of the samples with the contributions of individual astrophysical sources contributing more than 5% to the flux at any energy shown. Details and parameter values in the legend.

3. Flux from Dark Matter Annihilation and Decay

The spectral electron and positron fluxes per annihilation or decay have been calculated with PYTHIA 8.2 [15] for each studied annihilation/decay channel. These were used as input for the propagation calculation with DRAGON [16] to obtain the flux at Earth, with propagation conditions from Ref. [11]. For the local DM density, $\rho_0 = 0.3$ GeV/cm^3 is assumed and a NFW parametrization [17] for the halo shape, though the choice of the DM halo model has no strong impact given that the propagation range of electrons is limited. Fig. 2 shows the propagated spectra for the different annihilation and decay channels, demonstrating the increasing softness of the spectra in the order $e^+ + e^-$, $\mu^+ + \mu^-$, $\tau^+ + \tau^-$, $b + \bar{b}$. The lower panel shows the spectra for decay through

π+lepton channels, predicted for Skyrmion topological defect DM [18, 19]. Unlike the generic channels, this decay mode features different spectra in electron and positron. The $\pi^+ + e^-$ channel shows a hard spectrum in electrons but not positrons, giving the all-electron CALET measurement a larger contribution to the sensitivity.

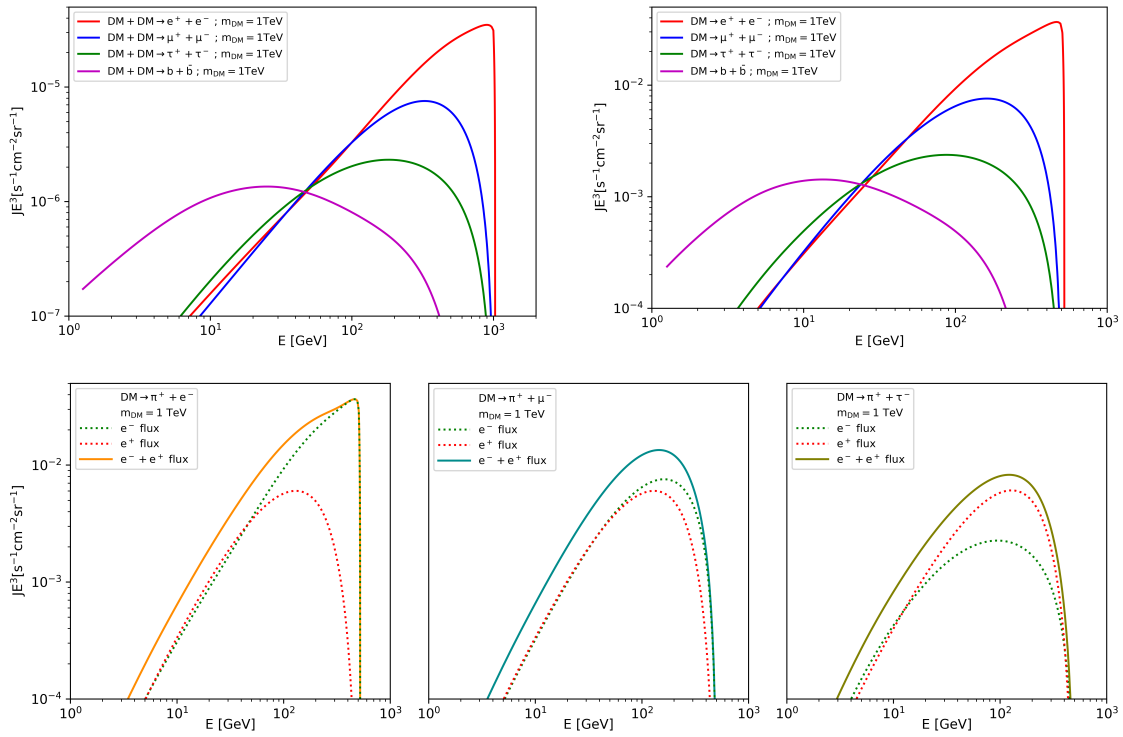

Figure 2: Top Left: Propagated flux from dark matter annihilation through generic channels for nominal cross section $\langle\sigma v\rangle = 3 \times 10^{-26}$ cm^3 s^{-1}. Top right: Propagated flux from dark matter decay through generic channels for nominal lifetime $\tau = 10^{28} s$. Bottom: Propagated flux from dark matter decay through π+lepton channels for nominal lifetime $\tau = 10^{28} s$ with separate electron and positron flux shown.

4. Method of Limit Calculation

To the fit of each sample to the CALET and AMS-02 data for which an example is shown in Fig. 1, the flux from DM annihilation/decay shown in Fig. 2 is added with a scale-factor increased in steps, and the fitting repeated at each step, readjusting all free parameters. When exceeding the 95%CL threshold, the step size is decreased and the process repeated until the step size falls below 1% of the scale-factor at the threshold, i.e. the limit scale-factor is determined at 1% precision. To avoid reporting a too stringent limit due to the fitting function having no unique minimum, the more robust gradient-descent Nelder-Mead algorithm is used if the faster BFGS algorithm (both implemented in SciPy.optimize [20]) fails to converge. Furthermore, the fitting is done with two sets of start parameters, the best parameters in the previous step and the original pure astrophysical model parameters, to avoid iterative convergence to local minima. Since the dependence of the flux on the cut-off energies $E_{cut(SNR)}$ and $E_{cut(pulsar)}$ does not allow for sufficiently fast calculation

to vary it continuously in the minimization [14], they are scanned on a logarithmic scale with 10 values per decade, with a maximum change of one order of magnitude from the original values. The relative limit is set where χ^2 increases by 3.841 from the base model fit, disfavoring the addition of DM at 95% CL, while an absolute limit can be set where χ^2 exceeds the 95% CL threshold for the fit's number of degrees of freedom, excluding the model including the DM flux. Examples are shown in Fig. 3. As the relative limit definition relies on the assumptions for the base model being true, only the absolute limits should be considered conservative in principle. However, by studying the variation of the astrophysical background and its influence on the limits in detail, as done herein by considering a large number of randomly generated samples, the reliability of the relative limits is enhanced so that they may be regarded as a valid constraint.

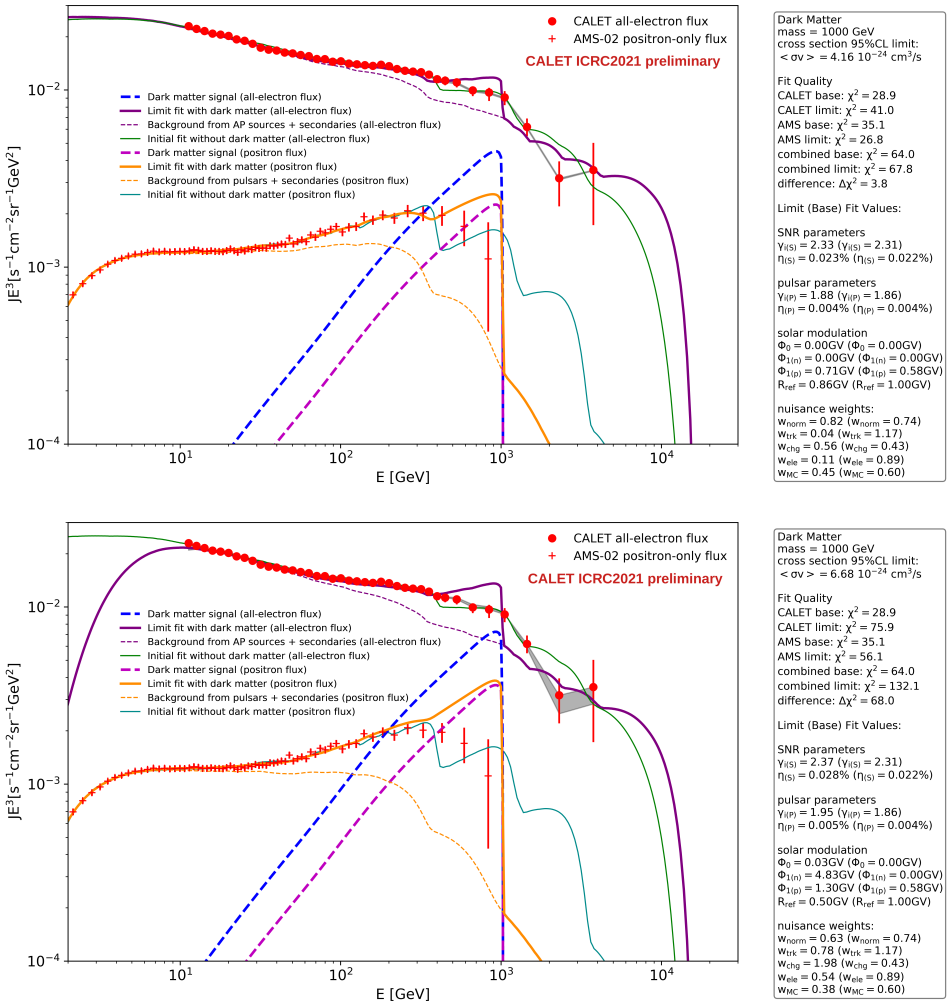

Figure 3: Top: Fit at the relative limit threshold for 1 TeV DM annihilation to $e^+ + e^-$ for the sample shown in Fig. 1, showing the added dark matter flux and the adaption of the background. Details given in the legend and fit parameters in the box on the right. Bottom: Same for absolute limit fit.

5. Limits on Dark Matter Annihilation and Decay Parameters

Fig. 4 shows as examples for the $DM + DM \rightarrow e^+ + e^-$ channel the obtained limits for the 80 samples as thin lines, and the worst (highest) limit as a thick line, on the left panel the absolute limit, and on the right panel the relative limit with the absolute limit as a dashed line for comparison. The lower panels show the factor between the highest limit and the limits from each of the samples, demonstrating that the relative limit has a much stronger dependence on the background than the absolute limit. Despite the wider spread, the worst relative limit is lower (stricter) than the absolute limit.

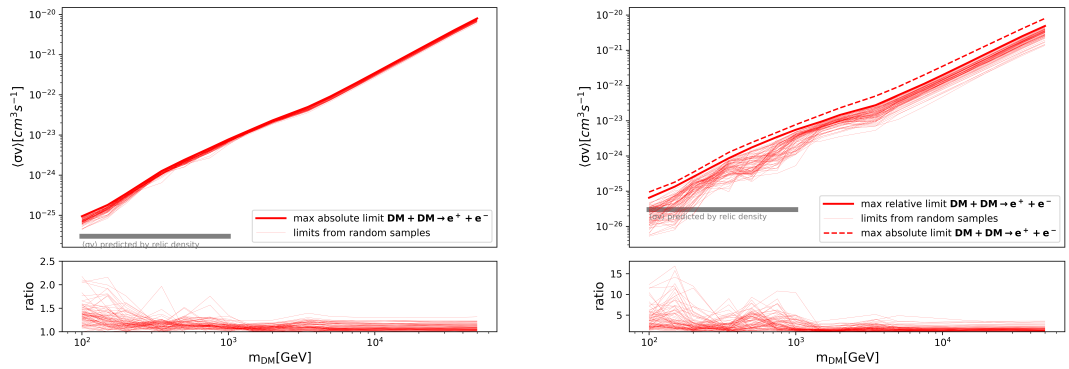

Figure 4: Left: Absolute 95% CL limits for annihilation to $e^+ + e^-$ for all 80 samples and highest limit, bottom panel shows ratio of individual sample limits to highest limit. Right: Same for relative limit fits.

The obtained limits on the annihilation cross-section are presented in Fig. 5, top panel, with a comparison to limits from γ-ray observation of dwarf galaxies with VERITAS [21] and Fermi-LAT [22]. The limits on DM lifetime shown in Fig. 5, middle panel are comparable to the most conservative EGRB limits from [23] which assume no astrophysical background, however based on specific astrophysical background models much stricter limits of O(10^{28} s) have been published (e.g. Ref [24]). Furthermore, limits on the lifetime of topological defect DM (Skyrmions [18]) decaying through a π+lepton channel [19] are shown in the bottom panel of Fig. 5.

6. Conclusions

From CALET all-electron and AMS-02 positron-only data, limits on DM lifetime (annihilation cross-section) have been calculated up to a DM mass of 100 TeV (50 TeV), which are comparable and, given the different sources of systematic uncertainty, complementing those from other messengers such as γ-rays and neutrinos. By using an astrophysical base model comprising random realizations of the individual SNR and pulsar sources within the galaxy, the effect of background variability and potential spectral structures from individual sources on the limits has been taken into account. Due to this, the presented stricter limits based on a relative χ^2 increase can be considered reliable constraints.

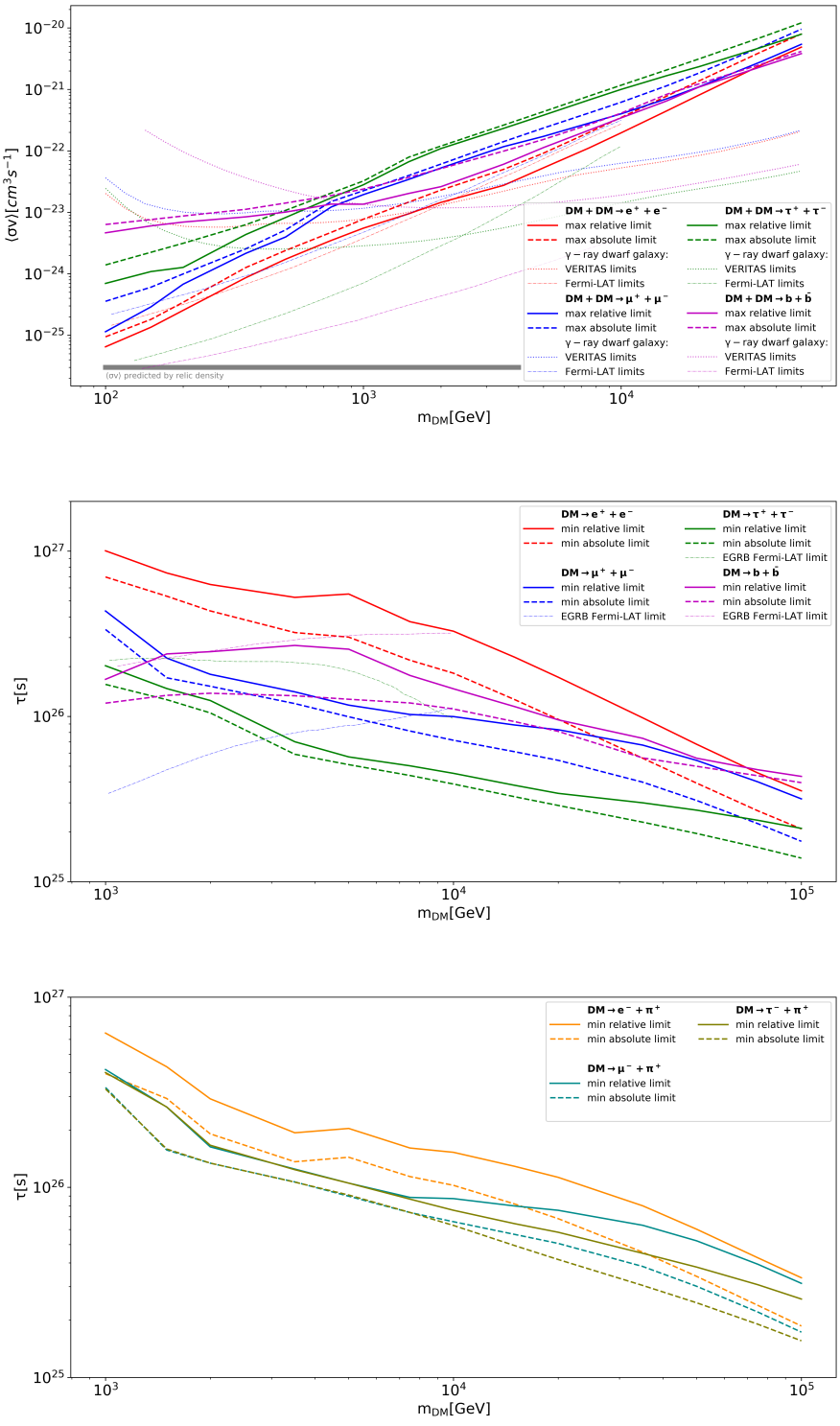

Figure 5: Top: 95% CL limits on $\langle \sigma v \rangle$ as a function of DM mass. For each DM mass the worst (highest) limit from the 80 samples is plotted. Middle: 95% CL limits on DM lifetime as a function of DM mass for generic decay channels. For each DM mass the worst (lowest) limit from the 80 samples is plotted. Bottom: 95% CL limits on DM lifetime as a function of DM mass for π+lepton decay channels. See text for a description of the comparison to other experiments.

Acknowledgments

We gratefully acknowledge JAXA's contributions to the development of CALET and to the operations onboard the International Space Station. The CALET effort in Italy is supported by ASI under Agreement No. 2013-018-R.0 and its amendments. The CALET effort in the United States is supported by NASA through Grants No. 80NSSC20K0397, No. 80NSSC20K0399, and No. NNH18ZDA001N-APRA18-0004. In Japan, this work is supported in part by JSPS Grant-in-Aid for Scientific Research (S) Grant No. 19H05608 and by JSPS Grant-in-Aid for Scientific Research (C) Grant No. JP21H05463.

References

[1] S. Torii, Y. Akaike, *PoS* **ICRC2021**, 105 (2021).
[2] M. Aguilar, *et al.*, *Phys. Rev. Lett.* **122**, 041102 (2019).
[3] H. Motz, Y. Asaoka, S. Torii, S. Bhattacharyya, *JCAP* **12**, 047 (2015).
[4] H. Motz, Y. Asaoka, S. Bhattacharyya, *PoS* **ICRC2019**, 533 (2019).
[5] H. Motz, H. Okada, Y. Asaoka, K. Kohri, *Phys. Rev. D* **102**, 083019 (2020).
[6] H. Motz, *SciPost Phys. Proc.* p. 035 (2023).
[7] K. M. Ferrière, *Rev. Mod. Phys.* **73**, 1031 (2001).
[8] K. P. Watters, R. W. Romani, *Astrophys. J.* **727**, 123 (2011).
[9] R. N. Manchester, G. B. Hobbs, A. Teoh, M. Hobbs, *Astron.J.* **129**, 1993 (2005).
[10] K. Asano, *et al.*, *Astrophys. J.* **926**, 5 (2022).
[11] H. Motz, *PoS* **ICRC2023**, 068 (2023).
[12] I. Cholis, D. Hooper, T. Linden, *Phys. Rev. D* **93**, 043016 (2016).
[13] O. Adriani, *et al.*, *Phys. Rev. Lett.* **120**, 261102 (2018).
[14] H. Motz, *PoS* **ICRC2023**, 067 (2023).
[15] T. Sjöstrand, *et al.*, *Computer Physics Communications* **191**, 159 (2015).
[16] D. Gaggero, *et al.*, *Phys.Rev.Lett.* **111**, 021102 (2013).
[17] J. F. Navarro, C. S. Frenk, S. D. M. White, *The Astrophysical Journal* **490**, 493 (1997).
[18] H. Murayama, J. Shu, *Phys. Lett. B* **686**, 162 (2010).
[19] E. D'Hoker, E. Farhi, *Phys. Lett. B* **134**, 86 (1984).
[20] P. Virtanen, *et al.*, *Nature Methods* **17**, 261 (2020).
[21] S. Archambault, *et al.*, *Phys. Rev. D* **95**, 082001 (2017).
[22] M. Ackermann, *et al.*, *Phys. Rev. Lett.* **115**, 231301 (2015).
[23] S. Ando, K. Ishiwata, *JCAP* **05**, 024 (2015).
[24] C. Blanco, D. Hooper, *JCAP* **03**, 019 (2019).

Full Author List: CALET Collaboration

O. Adriani[1,2], Y. Akaike[3,4], K. Asano[5], Y. Asaoka[5], E. Berti[2,6], G. Bigongiari[7,8], W.R. Binns[9], M. Bongi[1,2], P. Brogi[7,8], A. Bruno[10], N. Cannady[11,12,13], G. Castellini[6], C. Checchia[7,8], M.L. Cherry[14], G. Collazuol[15,16], G.A. de Nolfo[10], K. Ebisawa[17], A.W. Ficklin[14], H. Fuke[17], S. Gonzi[1,2,6], T.G. Guzik[14], T. Hams[11], K. Hibino[18], M. Ichimura[19], K. Ioka[20], W. Ishizaki[5], M.H. Israel[9], K. Kasahara[21], J. Kataoka[22], R. Kataoka[23], Y. Katayose[24], C. Kato[25], N. Kawanaka[20], Y. Kawakubo[14], K. Kobayashi[3,4], K. Kohri[26], H.S. Krawczynski[9], J.F. Krizmanic[12], P. Maestro[7,8], P.S. Marrocchesi[7,8], A.M. Messineo[8,27], J.W. Mitchell[12], S. Miyake[28], A.A. Moiseev[29,12,13], M. Mori[30], N. Mori[2], H.M. Motz[18], K. Munakata[25], S. Nakahira[17], J. Nishimura[17], S. Okuno[18], J.F. Ormes[31], S. Ozawa[32], L. Pacini[2,6], P. Papini[2], B.F. Rauch[9], S.B. Ricciarini[2,6], K. Sakai[11,12,13], T. Sakamoto[33], M. Sasaki[29,12,13], Y. Shimizu[18], A. Shiomi[34], P. Spillantini[1], F. Stolzi[7,8], S. Sugita[33], A. Sulaj[7,8], M. Takita[5], T. Tamura[18], T. Terasawa[5], S. Torii[3], Y. Tsunesada[35,36], Y. Uchihori[37], E. Vannuccini[2], J.P. Wefel[14], K. Yamaoka[38], S. Yanagita[39], A. Yoshida[33], K. Yoshida[21], and W.V. Zober[9]

[1]Department of Physics, University of Florence, Via Sansone, 1 - 50019, Sesto Fiorentino, Italy, [2]INFN Sezione di Firenze, Via Sansone, 1 - 50019, Sesto Fiorentino, Italy, [3]Waseda Research Institute for Science and Engineering, Waseda University, 17 Kikuicho, Shinjuku, Tokyo 162-0044, Japan, [4]JEM Utilization Center, Human Spaceflight Technology Directorate, Japan Aerospace Exploration Agency, 2-1-1 Sengen, Tsukuba, Ibaraki 305-8505, Japan, [5]Institute for Cosmic Ray Research, The University of Tokyo, 5-1-5 Kashiwa-no-Ha, Kashiwa, Chiba 277-8582, Japan, [6]Institute of Applied Physics (IFAC), National Research Council (CNR), Via Madonna del Piano, 10, 50019, Sesto Fiorentino, Italy, [7]Department of Physical Sciences, Earth and Environment, University of Siena, via Roma 56, 53100 Siena, Italy, [8]INFN Sezione di Pisa, Polo Fibonacci, Largo B. Pontecorvo, 3 - 56127 Pisa, Italy, [9]Department of Physics and McDonnell Center for the Space Sciences, Washington University, One Brookings Drive, St. Louis, Missouri 63130-4899, USA, [10]Heliospheric Physics Laboratory, NASA/GSFC, Greenbelt, Maryland 20771, USA, [11]Center for Space Sciences and Technology, University of Maryland, Baltimore County, 1000 Hilltop Circle, Baltimore, Maryland 21250, USA, [12]Astroparticle Physics Laboratory, NASA/GSFC, Greenbelt, Maryland 20771, USA, [13]Center for Research and Exploration in Space Sciences and Technology, NASA/GSFC, Greenbelt, Maryland 20771, USA, [14]Department of Physics and Astronomy, Louisiana State University, 202 Nicholson Hall, Baton Rouge, Louisiana 70803, USA, [15]Department of Physics and Astronomy, University of Padova, Via Marzolo, 8, 35131 Padova, Italy, [16]INFN Sezione di Padova, Via Marzolo, 8, 35131 Padova, Italy, [17]Institute of Space and Astronautical Science, Japan Aerospace Exploration Agency, 3-1-1 Yoshinodai, Chuo, Sagamihara, Kanagawa 252-5210, Japan, [18]Kanagawa University, 3-27-1 Rokkakubashi, Kanagawa, Yokohama, Kanagawa 221-8686, Japan, [19]Faculty of Science and Technology, Graduate School of Science and Technology, Hirosaki University, 3, Bunkyo, Hirosaki, Aomori 036-8561, Japan, [20]Yukawa Institute for Theoretical Physics, Kyoto University, Kitashirakawa Oiwake-cho, Sakyo-ku, Kyoto, 606-8502, Japan, [21]Department of Electronic Information Systems, Shibaura Institute of Technology, 307 Fukasaku, Minuma, Saitama 337-8570, Japan, [22]School of Advanced Science and Engineering, Waseda University, 3-4-1 Okubo, Shinjuku, Tokyo 169-8555, Japan, [23]National Institute of Polar Research, 10-3, Midori-cho, Tachikawa, Tokyo 190-8518, Japan, [24]Faculty of Engineering, Division of Intelligent Systems Engineering, Yokohama National University, 79-5 Tokiwadai, Hodogaya, Yokohama 240-8501, Japan, [25]Faculty of Science, Shinshu University, 3-1-1 Asahi, Matsumoto, Nagano 390-8621, Japan, [26]Institute of Particle and Nuclear Studies, High Energy Accelerator Research Organization, 1-1 Oho, Tsukuba, Ibaraki, 305-0801, Japan, [27]University of Pisa, Polo Fibonacci, Largo B. Pontecorvo, 3 - 56127 Pisa, Italy, [28]Department of Electrical and Electronic Systems Engineering, National Institute of Technology (KOSEN), Ibaraki College, 866 Nakane, Hitachinaka, Ibaraki 312-8508, Japan, [29]Department of Astronomy, University of Maryland, College Park, Maryland 20742, USA, [30]Department of Physical Sciences, College of Science and Engineering, Ritsumeikan University, Shiga 525-8577, Japan, [31]Department of Physics and Astronomy, University of Denver, Physics Building, Room 211, 2112 East Wesley Avenue, Denver, Colorado 80208-6900, USA, [32]Quantum ICT Advanced Development Center, National Institute of Information and Communications Technology, 4-2-1 Nukui-Kitamachi, Koganei, Tokyo 184-8795, Japan, [33]College of Science and Engineering, Department of Physics and Mathematics, Aoyama Gakuin University, 5-10-1 Fuchinobe, Chuo, Sagamihara, Kanagawa 252-5258, Japan, [34]College of Industrial Technology, Nihon University, 1-2-1 Izumi, Narashino, Chiba 275-8575, Japan, [35]Graduate School of Science, Osaka Metropolitan University, Sugimoto, Sumiyoshi, Osaka 558-8585, Japan, [36]Nambu Yoichiro Institute for Theoretical and Experimental Physics, Osaka Metropolitan University, Sugimoto, Sumiyoshi, Osaka 558-8585, Japan, [37]National Institutes for Quantum and Radiation Science and Technology, 4-9-1 Anagawa, Inage, Chiba 263-8555, Japan, [38]Nagoya University, Furo, Chikusa, Nagoya 464-8601, Japan, [39]College of Science, Ibaraki University, 2-1-1 Bunkyo, Mito, Ibaraki 310-8512, Japan

PoS(ICRC2023)1385